Nanoscale Research Letters
a SpringerOpen Journal

NANO EXPRESS **Open Access**

Numerical simulation of natural convection in a square enclosure filled with nanofluid using the two-phase Lattice Boltzmann method

Cong Qi, Yurong He[*], Shengnan Yan, Fenglin Tian and Yanwei Hu

Abstract

Considering interaction forces (gravity and buoyancy force, drag force, interaction potential force, and Brownian force) between nanoparticles and a base fluid, a two-phase Lattice Boltzmann model for natural convection of nanofluid is developed in this work. It is applied to investigate the natural convection in a square enclosure (the left wall is kept at a high constant temperature (T_H), and the top wall is kept at a low constant temperature (T_C)) filled with Al_2O_3/H_2O nanofluid. This model is validated by comparing numerical results with published results, and a satisfactory agreement is shown between them. The effects of different nanoparticle fractions and Rayleigh numbers on natural convection heat transfer of nanofluid are investigated. It is found that the average Nusselt number of the enclosure increases with increasing nanoparticle volume fraction and increases more rapidly at a high Rayleigh number. Also, the effects of forces on nanoparticle volume fraction distribution in the square enclosure are studied in this paper. It is found that the driving force of the temperature difference has the biggest effect on nanoparticle volume fraction distribution. In addition, the effects of interaction forces on flow and heat transfer are investigated. It is found that Brownian force, interaction potential force, and gravity-buoyancy force have positive effects on the enhancement of natural convective heat transfer, while drag force has a negative effect.

Keywords: Two phase Lattice Boltzmann model, Rayleigh number, Nanofluid, Natural convection

Background

Compared with common fluids such as water, nanofluid, using nanoscale particles dispersed in a base fluid, has an effect of enhancing the performance of natural convection heat transfer due to its high heat conductivity coefficient. Many researchers investigated nanoparticles and nanofluid in recent years. Wang et al. [1] synthesized stimuli-responsive magnetic nanoparticles and investigated the effect of nanoparticle fraction on its cleavage efficiency. Bora and Deb [2] developed a novel bioconjugate of stearic acid-capped maghemite nanoparticle (γ-Fe_2O_3) with bovine serum albumin. Guo et al. [3] produced magnetic nanofluids containing γ-Fe_2O_3 nanoparticles using a two-step method, measured their thermal conductivities and viscosity, and tested their convective heat transfer coefficients. Pinilla et al. [4]

investigated the growth of Cu nanoparticles in a plasma-enhanced sputtering gas aggregation-type growth region. Yang and Liu [5] produced a kind of stable nanofluid by surface functionalization of silica nanoparticles. Zhu et al. [6] developed a wet chemical method to produce stable CuO nanofluids. Nadeem and Lee [7] investigated the steady boundary layer flow of nanofluid over an exponential stretching surface. Wang and Fan [8] reviewed the nanofluid research in the last 10 years.

Natural convection is applied in many fields, and extensive researches have been performed. Oztop et al. [9] and Ho et al. [10] respectively investigated natural convection in partially heated rectangular enclosures and discussed the effects of viscosity and thermal conductivity of nanofluid on laminar natural convection heat transfer in a square enclosure by a finite-volume method. Saleh et al. [11] investigated heat transfer enhancement utilizing nanofluids in a trapezoidal enclosure by a finite difference approach. Ghasemi et al. [12], Santra et al. [13],

* Correspondence: rong@hit.edu.cn
School of Energy Science and Engineering, Harbin Institute of Technology, Harbin, 150001, China

and Aminossadati et al. [14] numerically simulated natural convection in a triangular enclosure and studied the behavior of natural convection heat transfer in a differentially heated square cavity, described a study on natural convection of a heat source embedded in the bottom wall of an enclosure, and used the SIMPLE algorithm to solve the governing equation. Kargar et al. [15] used computational fluid dynamics and an artificial neural network to investigate the cooling performance of two electronic components in an enclosure. Abu-Nada et al. [16] investigated the effect of variable properties on natural convection in enclosures filled with nanofluid, and the governing equations are solved by an efficient finite-volume method. Hwang et al. [17] investigated the thermal characteristics of natural convection in a rectangular cavity heated from below by Jang and Choi's model [18].

The Lattice Boltzmann method is a new way to investigate natural convection. Compared with the above traditional methods, the Lattice Boltzmann method has many merits including that boundary conditions can be conveniently dealt with, the transform between macroscopic and microscopic equations is easily achieved, the details of the fluid can be presented, and so on. In addition, nanofluid as the media can enhance heat transfer due to factors such as nanofluids having higher thermal conductivity and the nanoparticles in the fluid disturbing the laminar flow. Therefore, many researchers undertook investigations on the natural convection of nanofluids by the Lattice Boltzmann method. Barrios et al. [19] developed a Lattice Boltzmann model and applied it to investigate the natural convection of an enclosure with a partially heated left wall. Peng et al. [20] presented a simple a Lattice Boltzmann model without considering thermal diffusion, and this model is easily applied because it does not contain a gradient term. He et al. [21] proposed a new Lattice Boltzmann model which introduced an internal energy distribution function to simulate the temperature field, and the result has a good agreement with the benchmark solution. Nemati et al. [22] simulated the natural convection of a lid-driven flow filled with Cu-water, CuO-water, and Al_2O_3-water nanofluids and discussed the effects of nanoparticle volume fraction and Reynolds number on the heat transfer. Wang et al. [23] presented a Lattice Boltzmann algorithm to simulate the heat transfer of a fluid-solid fluid, and the result has a satisfactory agreement with the published data. Dixit et al. [24] applied the Lattice Boltzmann method to investigate the natural convection of a square cavity at high Rayleigh numbers. Peng et al. [25] developed a 3D incompressible thermal Lattice Boltzmann model for natural convection in a cubic cavity. The above Lattice Boltzmann

methods are all single-phase models, and the nanofluid was seen as a single-phase fluid without considering the interaction forces between nanoparticles and water. In addition, the effects of these interaction forces on heat transfer were disregarded.

There are few two-phase lattice Boltzmann models that consider the interaction forces between nanoparticles and a base fluid for natural convection in an enclosure. Xuan et al. [26] proposed a two-phase Lattice Boltzmann model to investigate sudden-start Couette flow and convection in parallel plate channels without researching the effect of forces on volume fraction distribution of nanoparticles. Because these forces were not investigated before our work, the effects of forces between water and nanoparticles on the fluid flow patterns were unknown. In addition, as we know, the nanoparticles in the fluid easily gather together and deposit, especially at high volume fraction. Hence, the nanoparticle distribution in the fluid flow is important for nanofluid application, which is another objective in our paper. However, the single-phase model cannot be used to investigate nanoparticle distribution. Furthermore, natural convection of a square enclosure (left wall kept at a high constant temperature (T_H), and top wall kept at a low constant temperature (T_C)) filled with nanofluid is not investigated in the published literatures. In this paper, a two-phase Lattice Boltzmann model is proposed and applied to investigate the natural convection of a square enclosure (left wall kept at a high constant temperature (T_H), and top wall kept at a low constant temperature (T_C)) filled with Al_2O_3-water nanofluid and the inhomogeneous distribution of nanoparticles in the square enclosure.

Methods
Lattice Boltzmann method
The density distribution function for a single-phase fluid is calculated as follows:

$$f_\alpha^\sigma(\boldsymbol{r} + \boldsymbol{e}_\alpha \delta_t, t + \delta_t) - f_\alpha^\sigma(\boldsymbol{r}, t)$$
$$= -\frac{1}{\tau_f^\sigma}\left[f_\alpha^\sigma(\boldsymbol{r}, t) - f_\alpha^{\sigma eq}(\boldsymbol{r}, t)\right] + \delta_t F_\alpha^{\sigma'} \qquad (1)$$

$$F_\alpha^{\sigma'} = \boldsymbol{G} \cdot \frac{(\boldsymbol{e}_\alpha - \boldsymbol{u}^\sigma)}{p} f_\alpha^{\sigma eq} \qquad (2)$$

where τ_f^σ is the dimensionless collision-relaxation time for the flow field, $\boldsymbol{e}_\alpha$ is the lattice velocity vector, the subscript α represents the lattice velocity direction, $f_\alpha^\sigma(r, t)$ is the distribution function of the nanofluid with velocity $\boldsymbol{e}_\alpha$ (along the direction α) at lattice position $\boldsymbol{r}$ and time $\boldsymbol{t}$, $f_\alpha^{\sigma eq}(r, t)$ is the local equilibrium distribution function, δ_t is the time step, δ_x is the lattice step, the order numbers

$\alpha = 1,\ldots,4$ and $\alpha = 5,\ldots,8$, respectively represent the rectangular directions and the diagonal directions of the lattice, $F_\alpha^{\sigma'}$ is the external force term in the direction of the lattice velocity without interparticle interaction, $G = -\beta(T_{nf} - T_0)\mathbf{g}$ is the effective external force, where $\mathbf{g}$ is the gravity acceleration, β is the thermal expansion coefficient, T_{nf} is the temperature of the nanofluid, and T_0 is the mean value of the high and low temperature of the walls.

A nanofluid is a two-phase fluid constituted by nanoparticles and a base fluid, and there are interaction forces (gravity and buoyancy force, drag force, interaction potential force, and Brownian force) between nanoparticles and the base fluid. Thus, the macroscopic density and velocity fields are simulated using the density distribution function by adding the forces term.

$$
\begin{aligned}
f_\alpha^\sigma(\mathbf{r} &+ \mathbf{e}_\alpha\delta_t, t + \delta_t) - f_\alpha^\sigma(\mathbf{r}, t) \\
&= -\frac{1}{\tau_f^\sigma}\left[f_\alpha^\sigma(\mathbf{r}, t) - f_\alpha^{\sigma eq}(\mathbf{r}, t)\right] \\
&+ \frac{2\tau_f^\sigma - 1}{2\tau_f^\sigma}\cdot\frac{F_\alpha^\sigma\delta_t\mathbf{e}_\alpha}{B_\alpha c^2} + \delta_t F_\alpha^{\sigma'}
\end{aligned}
\tag{3}
$$

where F_α^σ represents the total interparticle interaction forces, and B_α is one of the weight coefficients. $\frac{2\tau_f^\sigma - 1}{2\tau_f^\sigma}$ is a coefficient. Because the total interparticle interaction forces cannot be optionally added in the lattice Boltzmann equation, we introduce an unknown coefficient in the total interparticle interaction forces. In order to enable the lattice Boltzmann equation including the total interparticle interaction forces to recover to the Navier-Stokes equation, based on the mass and momentum conservation, we used multi-scale technique to deduce the unknown coefficient which is equal to $\frac{2\tau_f^\sigma - 1}{2\tau_f^\sigma}$. Due to the very long derivation process, we directly gave the final result in the paper.

The weight coefficient B_α is given as:

$$
B_\alpha = \begin{cases} 0 & \alpha = 0 \\ \dfrac{1}{3} & \alpha = 1,\ldots,4 \\ \dfrac{1}{12} & \alpha = 5,\ldots,8 \end{cases}
\tag{4}
$$

For the two-dimensional nine-velocity LB model (D2Q9) considered herein, the discrete velocity set for each component α is:

$$
\mathbf{e}_\alpha = \begin{cases} (0,0) & \alpha = 0 \\ c\left(\cos\left[(\alpha-1)\dfrac{\pi}{2}\right], \sin\left[(\alpha-1)\dfrac{\pi}{2}\right]\right) & \alpha = 1,2,3,4 \\ \sqrt{2}c\left(\cos\left[(2\alpha-1)\dfrac{\pi}{4}\right], \sin\left[(2\alpha-1)\dfrac{\pi}{4}\right]\right) & \alpha = 5,6,7,8 \end{cases}
\tag{5}
$$

The density equilibrium distribution function is chosen as follows:

$$
f_\alpha^{\sigma eq} = \rho^\sigma w_\alpha\left[1 + \frac{\mathbf{e}_\alpha\cdot\mathbf{u}^\sigma}{c_s^2} + \frac{(\mathbf{e}_\alpha\cdot\mathbf{u}^\sigma)^2}{2c_s^4} - \frac{u^{\sigma 2}}{2c_s^2}\right]
\tag{6}
$$

$$
w_\alpha = \begin{cases} \dfrac{4}{9} & \alpha = 0 \\ \dfrac{1}{9} & \alpha = 1,\ldots,4 \\ \dfrac{1}{36} & \alpha = 5,\ldots,8 \end{cases}
\tag{7}
$$

where $c_s^2 = \frac{c^2}{3}$ is the lattice's sound velocity, and w_α is the weight coefficient.

The macroscopic temperature field is simulated using the temperature distribution function.

$$
\begin{aligned}
T_\alpha^\sigma(\mathbf{r} &+ \mathbf{e}_\alpha\delta_t, t + \delta_t) - T_\alpha^\sigma(\mathbf{r}, t) \\
&= -\frac{1}{\tau_T^\sigma}\left[T_\alpha^\sigma(\mathbf{r}, t) - T_\alpha^{\sigma eq}(\mathbf{r}, t)\right]
\end{aligned}
\tag{8}
$$

where τ_T is the dimensionless collision-relaxation time for the temperature field.

The temperature equilibrium distribution function is chosen as follows:

$$
T_\alpha^{\sigma eq} = w_a T^\sigma\left[1 + 3\frac{\mathbf{e}_\alpha\cdot\mathbf{u}^\sigma}{c^2} + 4.5\frac{(\mathbf{e}_\alpha\cdot\mathbf{u}^\sigma)^2}{2c^4} - 1.5\frac{u^{\sigma 2}}{2c^2}\right]
\tag{9}
$$

In the case of no internal forces and external forces, the macroscopic temperature, density and velocity are respectively calculated as follows:

$$
T^\sigma = \sum_{\alpha=0}^{8} T_\alpha^\sigma
\tag{10}
$$

$$
\rho^\sigma = \sum_{\alpha=0}^{8} f_\alpha^\sigma
\tag{11}
$$

$$
\mathbf{u}^\sigma = \frac{1}{\rho^\sigma}\sum_{\alpha=0}^{8} f_\alpha^\sigma \mathbf{e}_\alpha
\tag{12}
$$

Considering the internal and external forces, the macroscopic velocities for nanoparticles and base fluid are modified to:

$$
\mathbf{u}_{pnew} = \mathbf{u}_p + \frac{F_p \Delta t \mathbf{e}_\alpha}{2\rho^\sigma}
\tag{13}
$$

$$
\mathbf{u}_{wnew} = \mathbf{u}_w + \frac{\Delta t F_W}{2L_x L_y \rho^w}
\tag{14}
$$

where F_p represents the total forces acting on the nanoparticles, F_w represents the total forces acting on the base fluid, and $L_x L_y$ represents the total number of lattices.
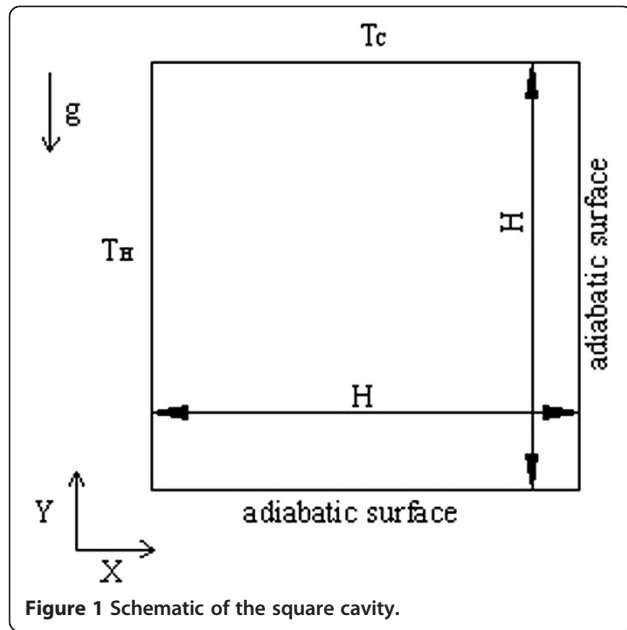
Figure 1 Schematic of the square cavity.

When the internal forces and external forces are considered, energy between nanoparticles and base fluid is exchanged, and the macroscopic temperature for nanoparticles and base fluid is then given as:

$$T_{new}^{\sigma} = T^{\sigma} + \delta_t \tau_T \frac{dT}{dt} = T^{\sigma} + \delta_t \tau_T \Phi_{\alpha\beta} \qquad (15)$$

where $\Phi_{\alpha\beta}$ is the energy exchange between nanoparticles and base fluid, $\Phi_{\alpha\beta} = \frac{h_{\alpha\beta}\left[T_{\beta}(x,t-\delta_t) - T_{\alpha}(x,t-\delta_t)\right]}{\rho_{\alpha} c_{p\alpha} a_{\alpha}}$, and $h_{\alpha\beta}$ is the convective heat transfer coefficient of the nanofluid.

The corresponding kinematic viscosity and thermal diffusion coefficients are respectively defined as follows:

$$\nu^{\sigma} = \frac{1}{3} c^2 \left(\tau_f^{\sigma} - \frac{1}{2} \right) \delta_t \qquad (16)$$

$$\chi^{\sigma} = \frac{1}{3} c^2 \left(\tau_T^{\sigma} - \frac{1}{2} \right) \delta_t \qquad (17)$$

The dimensionless collision-relaxation times τ_f and τ_T are respectively given as follows:

$$\tau_f^{\sigma} = 0.5 + \frac{MaH\sqrt{3Pr}}{c^2 \delta_t \sqrt{Ra}} \qquad (18)$$

Table 1 Thermo-physical properties of water and Al$_2$O$_3$ [29]

Physical properties	Fluid phase (H$_2$O)	Nanoparticles (Al$_2$O$_3$)
ρ (kg/m^3)	997.1	3970
c_p (J/kg k)	4179	765
ν (m^2/s)	0.001004	-
k (W/m/K)	0.613	25

Table 2 Comparison of the mean Nusselt numbers with different grids ($Ra = 1 \times 10^5$, $Pr = 0.7$)

Physical properties	128 × 128	192 × 192	256 × 256	320 × 320	Literature [30]
Nu_{avg}	4.5466	4.5251	4.5220	4.5218	4.5216

$$\tau_T^{\sigma} = 0.5 + \frac{3\nu}{Prc^2\delta t} \qquad (19)$$

where Ma = 0.1, H = 1, c = 1, δt = 1, and the other parameters equations are given as follows:

$$Pr = \frac{\nu}{\alpha} = \frac{c_p \mu}{k} \qquad (20)$$

$$\nu = \frac{\mu}{\rho} \qquad (21)$$

From Equations 18 and 19, the collision-relaxation time for the flow field and the temperature field can be calculated. For water phase, the τ_f collision-relaxation times are respectively 0.51433 and 0.501433 at Ra = 10^3 and Ra = 10^5, and the collision-relaxation time τ_T is 0.5. For nanoparticle phase, the τ_f collision-relaxation times are respectively 0.50096 and 0.500096 at Ra = 10^3 and Ra = 10^5, and the collision-relaxation time τ_T is 0.500025.

Interaction forces between base fluid and nanoparticles

As noted before, a nanofluid is, in reality, a kind of two-phase fluid. There are interaction forces between liquid and nanoparticles which affect the behavior of the nanofluid. The external forces include gravity and buoyancy forces F_H, and the interparticle interaction forces include drag force (Stokes force) F_D, interaction potential F_A, and Brownian force F_B. We introduce them as follows.
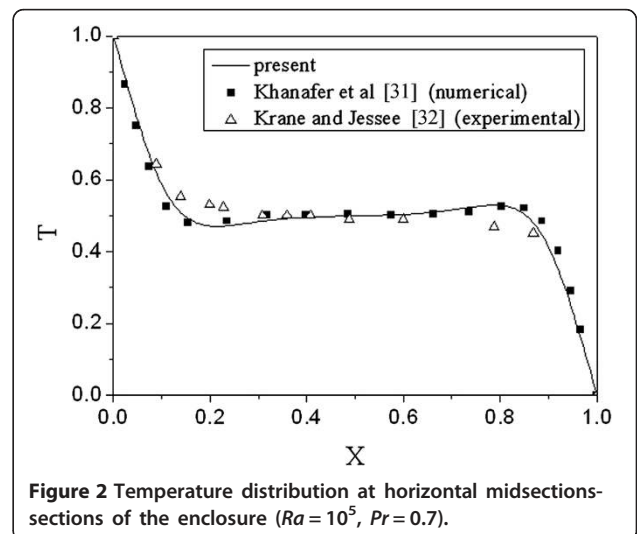

Figure 2 Temperature distribution at horizontal midsections-sections of the enclosure ($Ra = 10^5$, $Pr = 0.7$).

Table 3 Comparison of average Nusselt numbers with other published data ($Pr = 0.7$)

	$Ra = 10^3$	$Ra = 10^4$	$Ra = 10^5$	$Ra = 10^6$
Present work	1.118	2.247	4.522	8.808
D'Orazio et al. [33]	1.117	2.235	4.504	8.767
De Vahl Davis [34]	1.118	2.243	4.519	8.800
Khanafer et al. [31]	1.118	2.245	4.522	8.826

The gravity and buoyancy force is given as:

$$F_H = -\frac{4\pi a^3}{3} g \Delta \rho' \qquad (22)$$

where a is the radius of a nanoparticle, and $\Delta \rho'$ is the mass density difference between the suspended nanoparticle and the base fluid.

The drag force (Stokes force) is given as:

$$F_D = -6\pi \mu a \Delta u \qquad (23)$$

where μ is the viscosity of the fluid, and Δu is the velocity difference between the nanoparticle and the base fluid.

The interaction potential is presented as [27]:

$$V_A = -\frac{1}{6} A \left(\frac{2a^2}{L_{cc}^2 - 4a^2} + \frac{2a^2}{L_{cc}^2} + \frac{L_{cc}^2 - 4a^2}{L_{cc}^2} \right) \qquad (24)$$

where A is the Hamaker constant, and L_{cc} is the center-to-center distance between particles.

The interaction potential force is shown as:

$$F_A = \sum_{i=1}^{8} n_i \frac{\partial V_A}{\partial r_i} \qquad (25)$$

where n_i is the number of the particles within the adjacent lattice i, $n_i = \rho^\sigma V / m^\sigma$, m^σ is the mass of a single nanoparticle, and V is the volume of a single lattice.

The Brownian force is calculated as [28]:

$$F_B = G_i \sqrt{\frac{C}{dt}} \qquad (26)$$

where G_i is a Gaussian random number with zero mean and unit variance, which is obtained from a program written by us, and $C = 2\gamma k_B T = 2 \times (6\pi\eta a) k_B T$, γ is the surface tension, k_B is the Boltzmann constant, T is the absolute temperature, and η is the dynamic viscosity.

The total per unit volume forces acting on nanoparticles of a single lattice is:

$$F_p = n(F_H + F_D + F_A + F_B)/V \qquad (27)$$

where n is the number of the particles in the given lattice, and V is the lattice volume.

In a nanofluid, the forces acting on the base fluid are mainly drag force and Brownian force. Thus the force acting on the base fluid in a given lattice is:

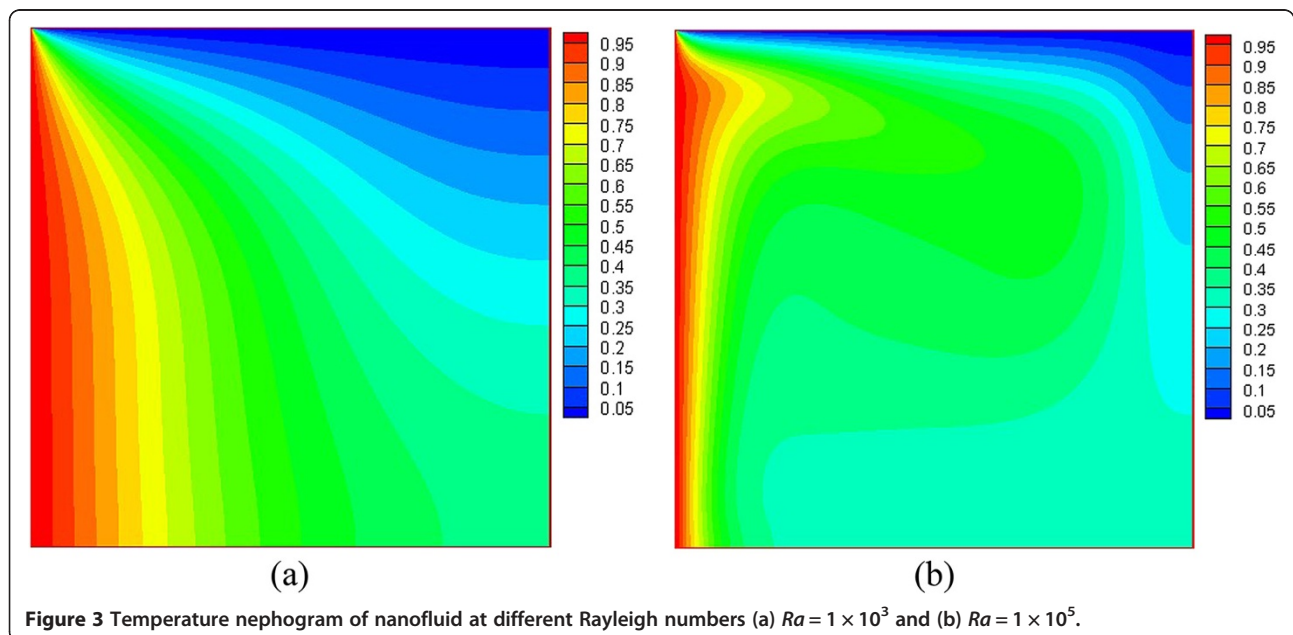$$F_w = -n(F_D + F_B) \qquad (28)$$

Figure 3 Temperature nephogram of nanofluid at different Rayleigh numbers (a) $Ra = 1 \times 10^3$ and (b) $Ra = 1 \times 10^5$.

Results and discussion

The two-phase Lattice Boltzmann model is applied to simulate the natural convection heat transfer in a square cavity which is shown in Figure 1. The square cavity is filled with the Al_2O_3-water nanofluid. The thermophysical properties of water and Al_2O_3 are given in Table 1. The height and the width of the enclosure are both H. The left wall is kept at a high constant temperature (T_H), and the top cold wall is kept at a low constant temperature (T_C). The boundary conditions of the other walls (right wall and bottom wall) are all adiabatic. The initial conditions for the four walls are given as follows:

$$\begin{cases} x=0 & \boldsymbol{u}=0, \quad T=1; \quad & x=1 \quad \boldsymbol{u}=0, \quad \partial T/\partial y=0 \\ y=0 & \boldsymbol{u}=0, \quad \partial T/\partial y=0; \quad & y=1 \quad \boldsymbol{u}=0, \quad T=0 \end{cases}$$

(29)

In the simulation, a non-equilibrium extrapolation scheme is adopted to deal with the boundary, and the criteria of the program convergence for the flow field and the temperature field are respectively given as follows:

$$\text{Error}_1 = \frac{\sqrt{\sum_{i,j}\left\{\left[u_x^\sigma(i,j,t+\delta_t)-u_x^\sigma(i,j,t)\right]^2+\left[u_y^\sigma(i,j,t+\delta_t)-u_y^\sigma(i,j,t)\right]^2\right\}}}{\sqrt{\sum_{i,j}\left[u_x^\sigma(i,j,t+\delta_t)^2+u_y^\sigma(i,j,t+\delta_t)^2\right]}} < \varepsilon_1$$

(30)

$$\text{Error}_2 = \frac{\sqrt{\sum_{i,j}\left[T^\sigma(i,j,t+\delta_t)-T^\sigma(i,j,t)\right]^2}}{\sqrt{\sum_{i,j}T^\sigma(i,j,t+\delta_t)^2}} < \varepsilon_2$$

(31)

where ε is a small number, for example, for Ra = 1×10^3, $\varepsilon_1 = 10^{-6}$, and $\varepsilon_2 = 10^{-6}$. About 2 weeks is needed to achieve the equilibrium state for the low Rayleigh number (Ra = 1×10^3), and about 1 month for the high Rayleigh number (Ra = 1×10^5).
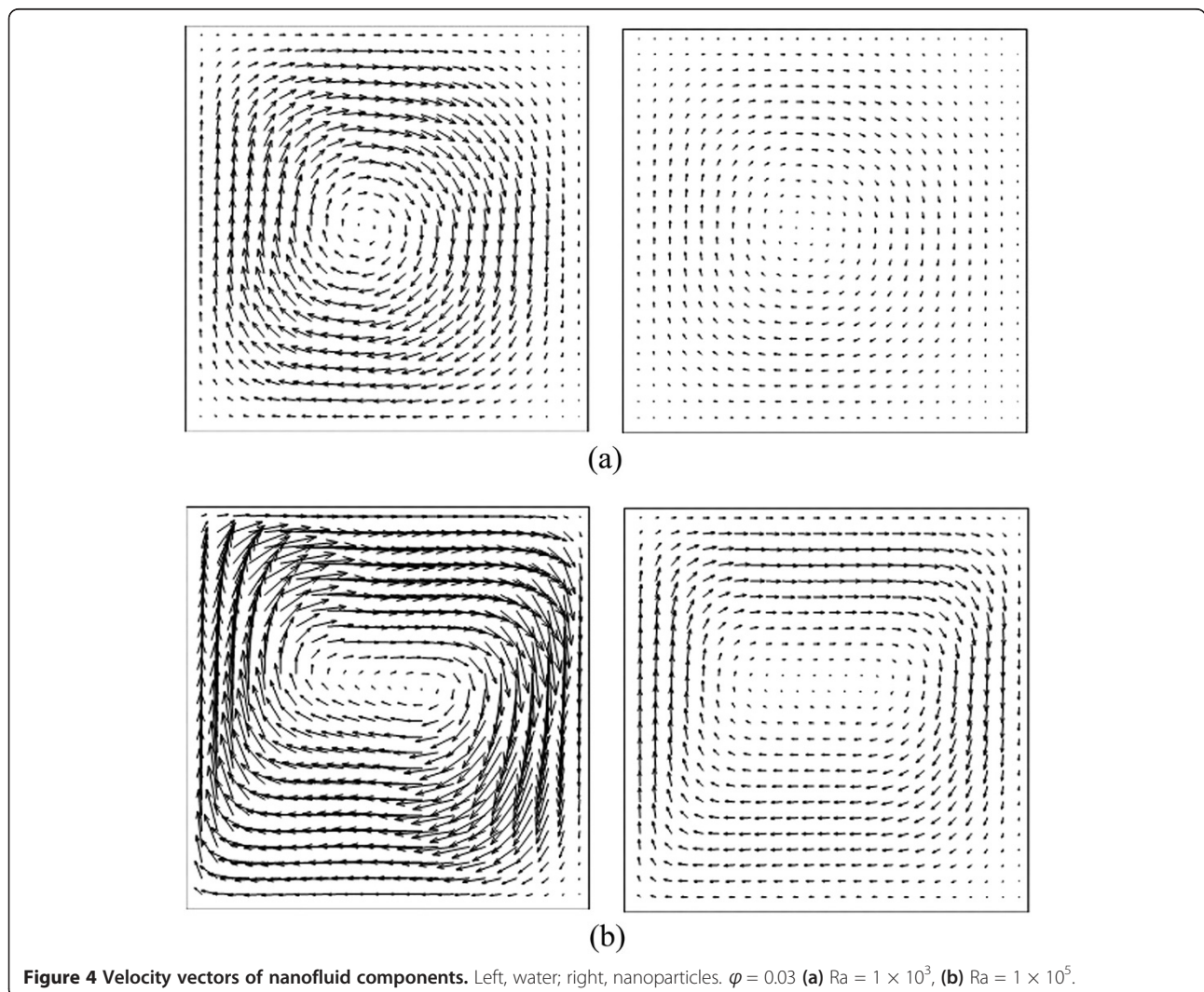

Figure 4 Velocity vectors of nanofluid components. Left, water; right, nanoparticles. φ = 0.03 **(a)** Ra = 1×10^3, **(b)** Ra = 1×10^5.

Table 4 Comparison of different forces ($Ra = 10^5$, $\varphi = 0.03$)

	Forces						
	F_S	F_A	F_{Bx}	F_{By}	F_H	F_{Dx}	F_{Dy}
Minimum	−6E−06	−3.2E−19	−5E−13	2E−14	−9E−19	−8E−16	−1.6E−15
Maximum	6E−06	−2E−20	5E−13	2E−13	−1E−19	1.2E−15	1.6E−15

The Nusselt number can be expressed as:

$$\text{Nu} = \frac{hH}{k_{nf}}. \tag{32}$$

The heat transfer coefficient is computed from:

$$h = \frac{q_w}{T_H - T_L}. \tag{33}$$

The thermal conductivity of the nanofluid is defined by:

$$k_{nf} = -\frac{q_w}{\partial T / \partial x}. \tag{34}$$

Substituting Equations 33 and 34 into Equation 32, the local Nusselt number along the left wall can be written as:

$$\text{Nu} = -\left(\frac{\partial T}{\partial x}\right) \cdot \frac{H}{T_H - T_L}. \tag{35}$$

The average Nusselt number is determined from:

$$\text{Nu}_{\text{avg}} = \int_0^1 \text{Nu}(y)dy. \tag{36}$$

In order to perform a grid independence test and validate the Lattice Boltzmann model proposed in this work, we used another square enclosure, because there are exact solutions for this square enclosure. The left wall is kept at a high constant temperature (T_H), and the right wall is kept at a low constant temperature (T_C). The boundary conditions of the other walls (top wall and bottom wall) are all adiabatic, and the other conditions are the same as those in Figure 1.

As shown in Table 2, the grid independence test is performed in a square enclosure using successively sized grids, 128 × 128, 192 × 192, 256 × 256, and 320 × 320 at $Ra = 1 \times 10^5$, $Pr = 0.7$. It can be seen from Table 2 that there is a bigger difference between the result obtained with grid sizes 128 × 128 and 192 × 192 and the result available from the literature [30] than when compared with the result obtained with grids 256 × 256 and 320 × 320. In addition, the result with grid 256 × 256 and the result with grid 320 × 320 are very close. In order to accelerate the numerical simulation, a grid size of 256 × 256 was chosen as a suitable one which can guarantee a grid-independent solution.

In order to validate the Lattice Boltzmann model proposed in this work, the temperature distribution at midsections of the enclosure at $Ra = 1 \times 10^5$, $Pr = 0.7$ is compared with the numerical results from Khanafer et al. [31] and experimental results from Krane et al. [32] in Figure 2. It can be seen that the results of this paper have a good agreement with those numerical [31]
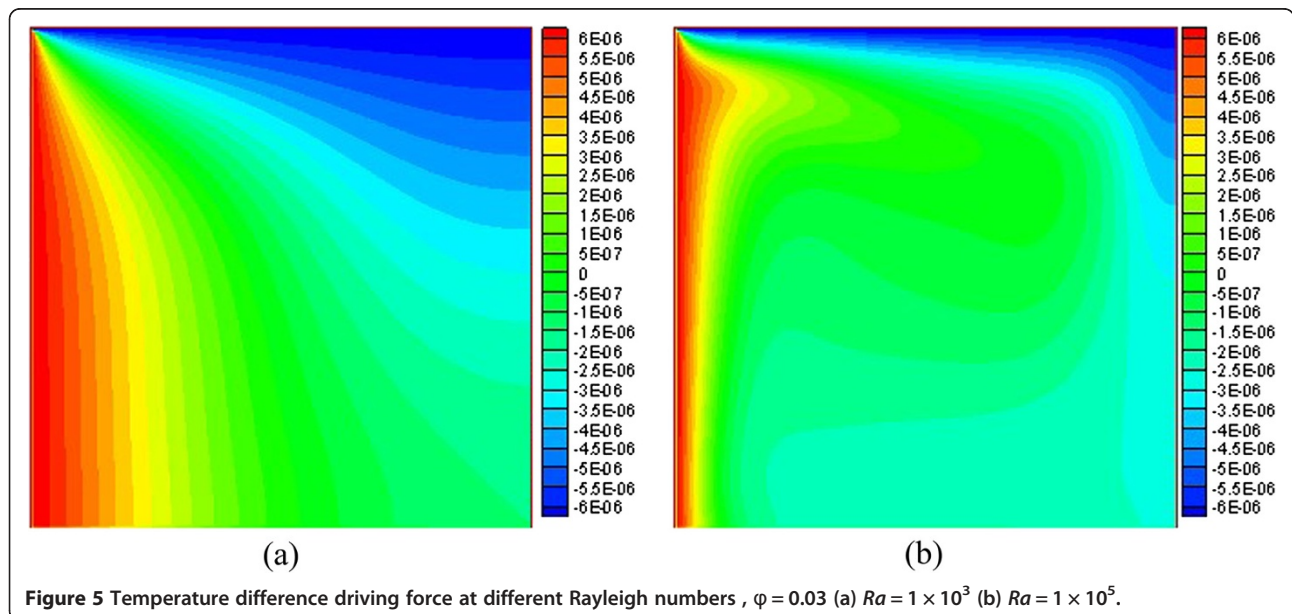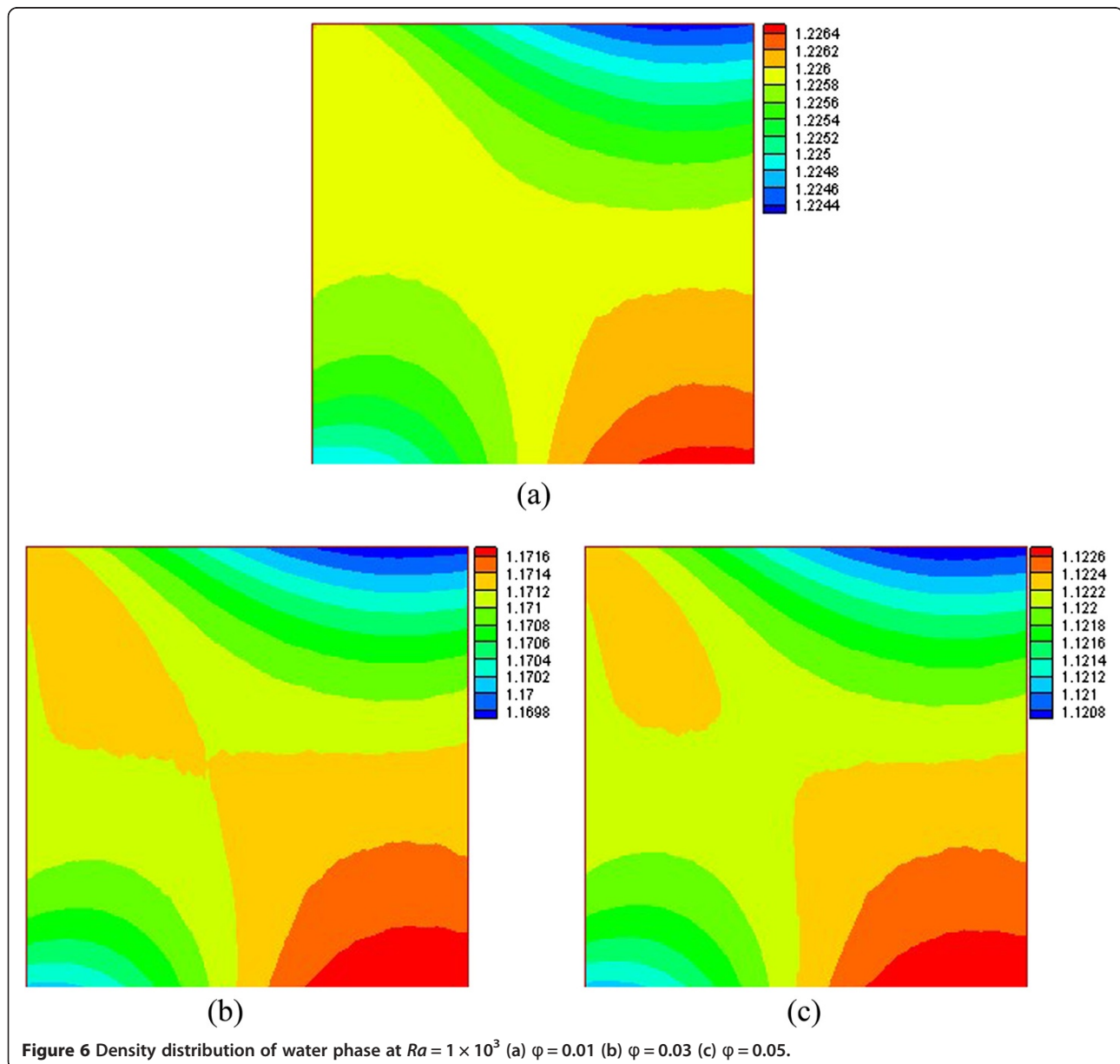

Figure 5 Temperature difference driving force at different Rayleigh numbers , $\varphi = 0.03$ (a) $Ra = 1 \times 10^3$ (b) $Ra = 1 \times 10^5$.

and experimental [32] results. They are closer to the experimental [32] than the numerical [31] results. In addition, the Nusselt number results at different Rayleigh numbers of this paper are compared with other published literature listed in Table 3, and it can be seen that the results are in good agreement.

Due to the temperature balance between water and nanoparticles, the temperature nephogram of water and nanoparticles for each of the nanoparticle fractions are identical. The temperature nephograms of nanofluid at $Ra = 1 \times 10^3$ and $Ra = 1 \times 10^5$ are presented in Figure 3. It can be seen that isotherms are more crooked with the higher Rayleigh number, which denotes

that the heat transfer characteristic transforms from conduction to convection.

Because there are fewer nanoparticles than water molecules, and the drag force of nanoparticles on water is small, the velocity vectors of nanofluid with different nanoparticle fractions have such small differences that it is difficult to distinguish them. However, the differences can be observed in the Nusselt number distribution. For this reason, only the velocity vectors of nanofluid components with $\phi = 0.03$ at different Rayleigh numbers are given as an example in Figure 4. Separating the nanofluid into its two constitutive components, it can be seen that the velocity vectors of the

Figure 6 Density distribution of water phase at $Ra = 1 \times 10^3$ **(a)** $\varphi = 0.01$ **(b)** $\varphi = 0.03$ **(c)** $\varphi = 0.05$.

water component are larger than those of the nanoparticle component due to the law of conservation of momentum. The velocity difference between the water component and the nanoparticle component gives rise to the drag force. In addition, it can be seen that velocity increases with Rayleigh number, which can also explain that the heat transfer characteristic transforms from conduction to convection.

Driving force and interaction forces have a big effect on nanoparticle volume fraction distribution and the flow and heat transfer characteristics of the nanofluid. The main driving force in this work is the temperature difference. Interaction forces between nanoparticles and base fluid include gravity-buoyancy force, drag force, interaction potential force, and Brownian force. In order to compare the effects of these forces, the ranges of them are presented in Table 4. We used double-precision variables in our code. From Table 4, we can find that the temperature difference driving force F_S is much bigger than the other forces (interaction forces between nanoparticles and base fluid). The driving force has the greatest effect on nanoparticle volume fraction distribution, and the effects of other forces on nanoparticle volume fraction distribution can be ignored in this case. However, these other forces play an important role in the flow and heat transfer of the nanofluid. Apart

Figure 7 Density distribution of water phase at $Ra = 1 \times 10^5$ **(a)** φ = 0.01 **(b)** φ = 0.03 **(c)** φ = 0.05.
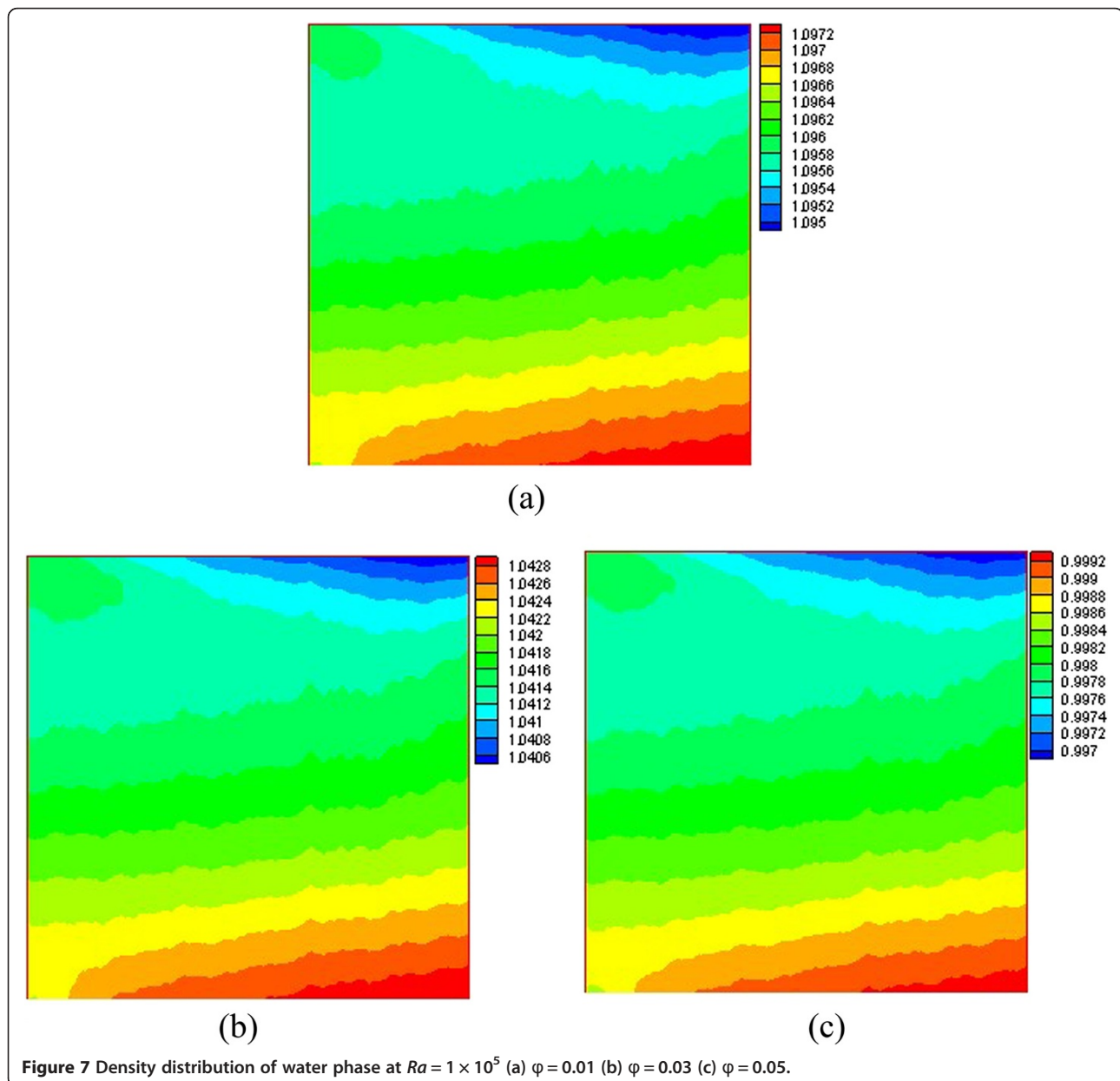
from the temperature difference driving force, the Brownian force is much larger than other forces, which is different from other two-phase fluids. For this reason, the Brownian force can enhance the heat transfer of the nanofluid by disturbing the flow boundary layer and the thermal boundary layer. Drag force comes about due to the velocity difference between nanoparticles and water molecules, and the nanoparticles in the water decrease the velocity of nanofluid in the enclosure, which in turn attenuates the natural convection of nanofluid in the enclosure. The interaction potential force prevents the nanoparticles from gathering together and keeps the nanoparticles dispersed in the water. In addition to the above forces, there is the gravity-buoyancy force, that is, the sum of gravity of

the nanoparticles themselves and the buoyancy force of the water. The gravity-buoyancy force and temperature difference driving force together give rise to the velocity vectors of the nanofluid within the enclosure. In summary, Brownian force, interaction potential force, and gravity-buoyancy force contribute to the enhanced natural convective heat transfer, while drag force contributes to the attenuation of heat transfer.
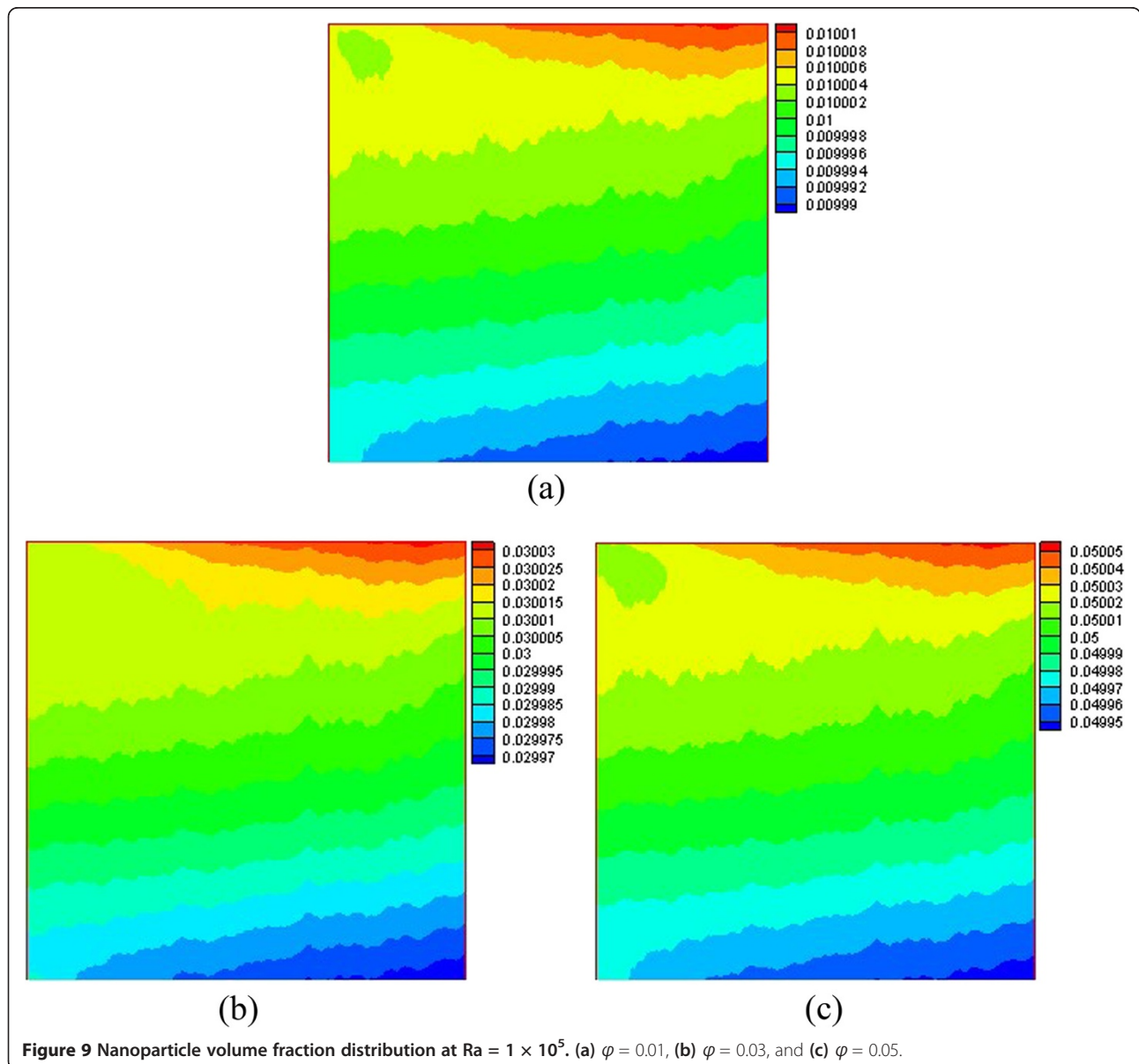
The temperature difference driving force distribution in the square at different Rayleigh numbers is given in Figure 5. From Figure 5, we can see that the temperature difference driving force along the left wall (high temperature) and the top wall (low temperature) is high. Its direction along the high-temperature wall is upward, and that along the low-temperature wall is

Figure 8 Nanoparticle volume fraction distribution at Ra = 1 × 10³. (a) φ = 0.01, (b) φ = 0.03, and (c) φ = 0.05.
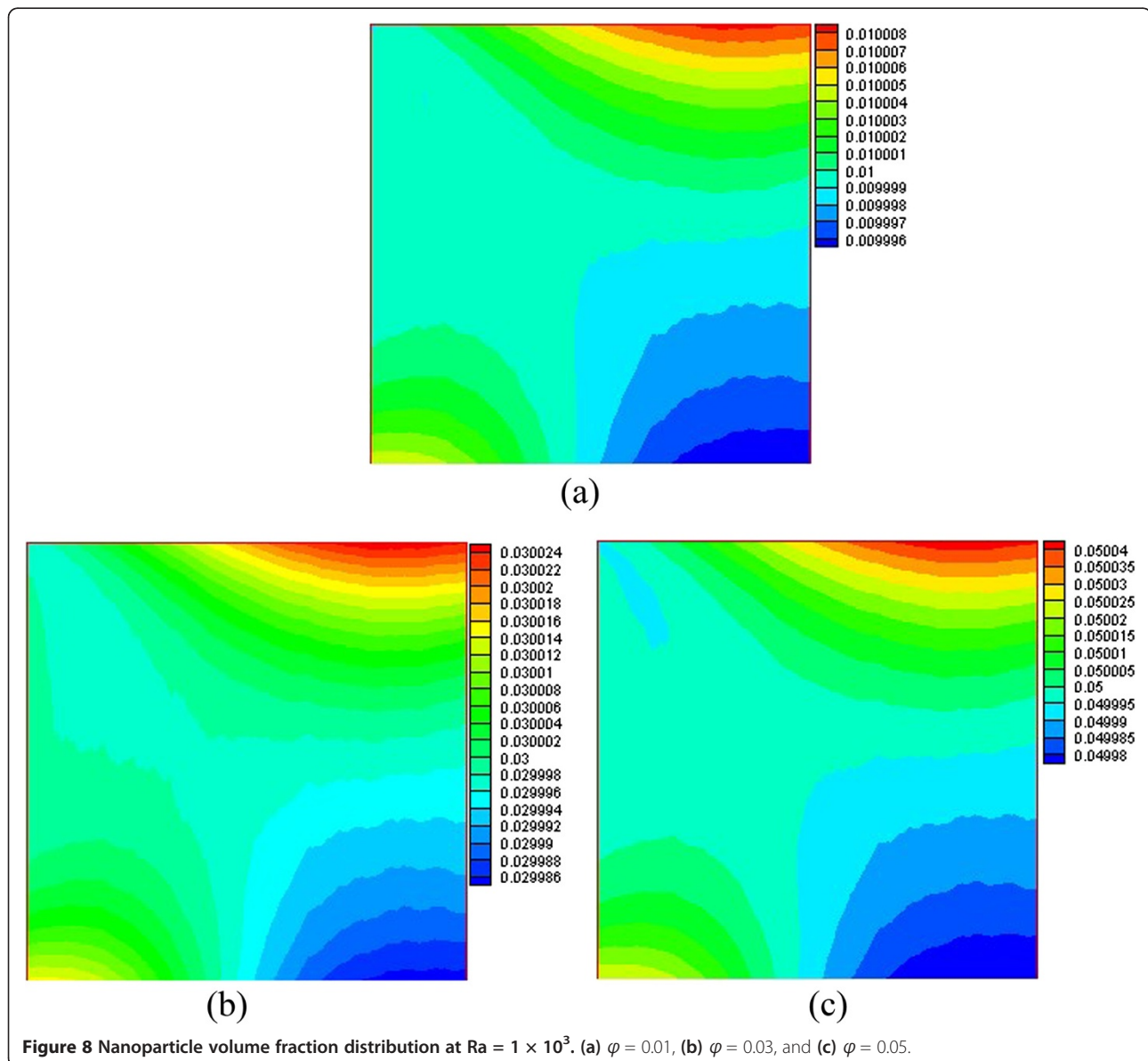
downward, while the temperature difference driving force in other regions far away from the two walls (left wall and top wall) is small. From Figure 3, it can be seen that the temperature gradient near the left wall and the top wall is higher than that in other regions, which causes a high temperature difference driving force near there. Similarly, the temperature gradient in other regions is small, causing only a low temperature difference driving force in that vicinity. In addition, it can be seen that the same driving force line at a high Rayleigh number becomes more crooked than that at a low Rayleigh number. This is because the driving force is caused by the temperature difference (temperature gradient); a bigger temperature gradient

causes the same driving force line to become more crooked. It can be seen from Figure 3 that isotherms are more crooked at a higher Rayleigh number, and the isotherm changes correspond to the changes of temperature gradient. Thus, the conclusion that the same driving force line at a high Rayleigh number becomes more crooked than that that at a low Rayleigh number is obtained.

Figures 6 and 7 give the density distribution of the water phase at $Ra = 1 \times 10^3$ and $Ra = 1 \times 10^5$. For a low Rayleigh number ($Ra = 1 \times 10^3$), when the water near the left wall is heated, its density decreases and flows upward, so the density of water near the top right corner also becomes smaller. Then when the

Figure 9 Nanoparticle volume fraction distribution at Ra = 1 × 10^5. (a) φ = 0.01, **(b)** φ = 0.03, and **(c)** φ = 0.05.

water is cooled by the top wall, the density of the water becomes larger. Then the denser water flows downward to the lower right corner, and so, the density of water in the lower right corner is larger than that in other regions. Because the temperature gradient (corresponding to the temperature difference driving force) is small and the temperature is high in the lower left corner, the density of water in the lower left corner is thus low. For a high Rayleigh number (Ra = 1 × 10⁵), the temperature gradient and the corresponding driving force become larger, then the lower-density water, including that in the lower left corner, rises to the top right corner. The denser water is cooled by the top wall and flows downward to the lower right corner, and the area where the denser water in the lower right corner becomes larger.

Figures 8 and 9 respectively present the nanoparticle distribution of nanofluid with volume fractions at Ra = 1 × 10³ and Ra = 1 × 10⁵. For a low Rayleigh number (Ra = 1 × 10³), the driving force along the left wall is upward, and many nanoparticles are driven to the top right corner, which contributes to the high nanoparticle volume fraction in the top right corner. However, the temperature gradient in the lower left corner is small and causes a correspondingly small temperature difference driving force. Thus, many nanoparticles are left in the lower left corner, which contributes to the high nanoparticle volume fraction in the lower left corner. There is a large temperature gradient in the lower right corner, and the large driving force displaces the nanoparticles off the lower

right corner, which contributes to the low nanoparticle volume fraction in the lower right corner. For a high Rayleigh number (Ra = 1 × 10⁵), the convection heat transfer is enhanced and the velocity of the nanofluid becomes larger, and the temperature gradient and the corresponding driving force become bigger. Thus, many nanoparticles from the bottom are driven to the top by the driving force, which contributes to the low nanoparticle volume fraction at the bottom and a high nanoparticle volume fraction at the top. In addition, we can see that the nanoparticle volume fraction distribution is opposite to that of the water-phase density distribution. From Table 4, we can see that the temperature difference driving force is the biggest one, and the changes of the water-phase density and the inhomogeneous nanoparticle distribution are mainly due to the driving force. Through the above analysis, it is found that the nanoparticles migrate to locations where the water density is small, and thus, the conclusion that the nanoparticle volume fraction distribution is opposite to that of the water-phase density distribution is obtained.

It is also found that almost all the isolines behave with oscillations in Figures 6, 7, 8, 9, but smooth isolines are given in Figures 3 and 5. Due to the ruleless Brownian movement of nanoparticles, it is difficult for nanofluid to achieve a complete equilibrium state, which is the difference compared with other common two-phase fluids. In order to expediently judge the equilibrium state and save time, we choose the temperature equilibrium states of water phase and nanoparticle phase as the whole nanofluid equilibrium state in the computation. When
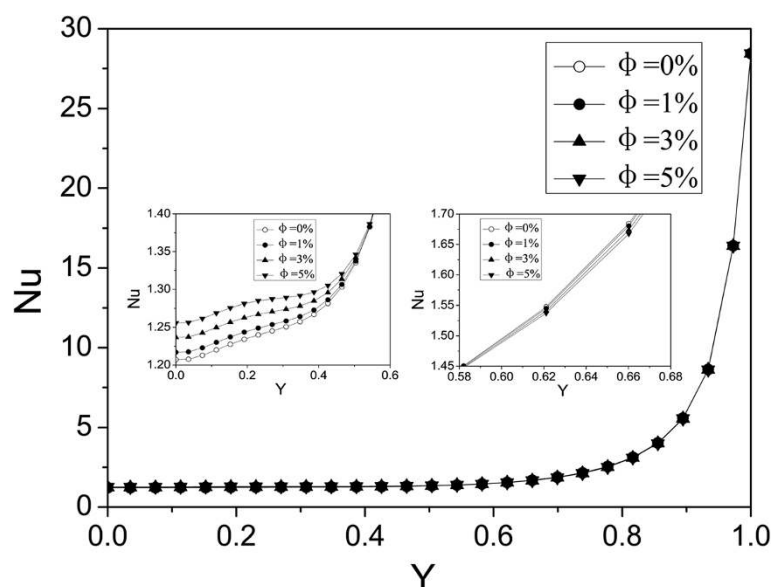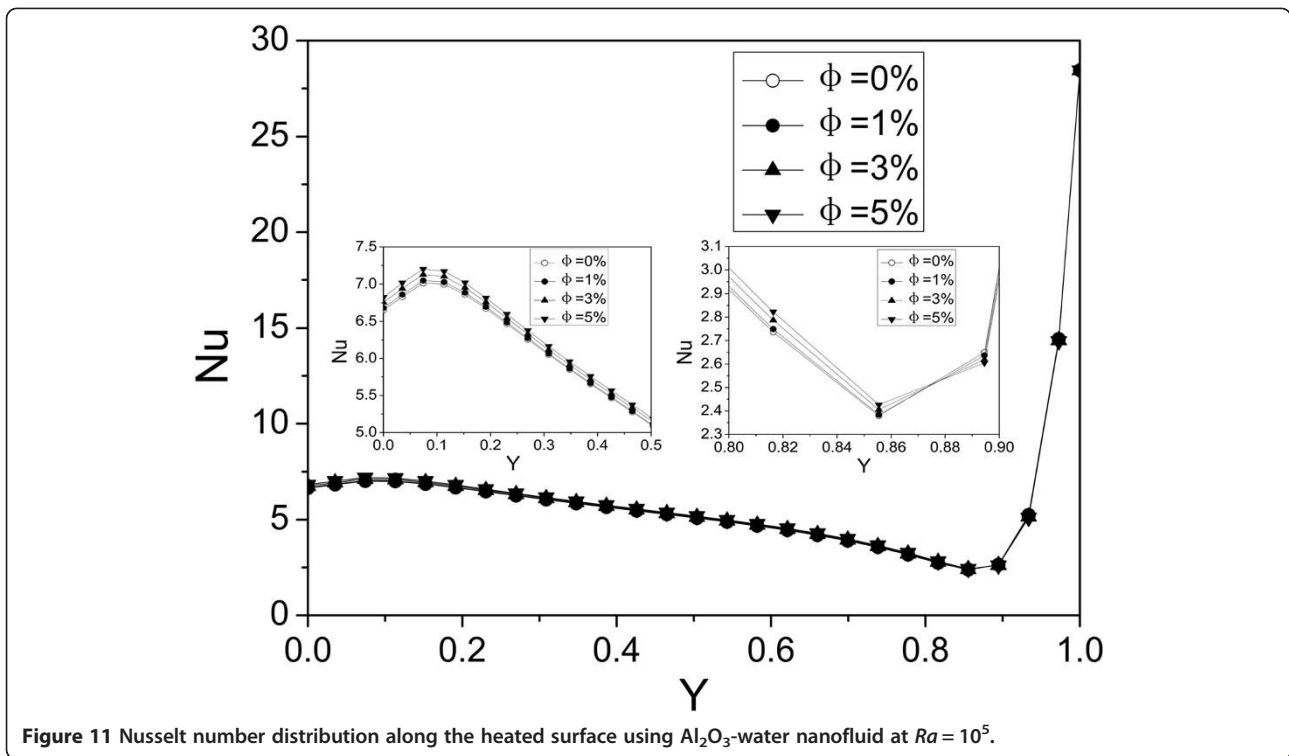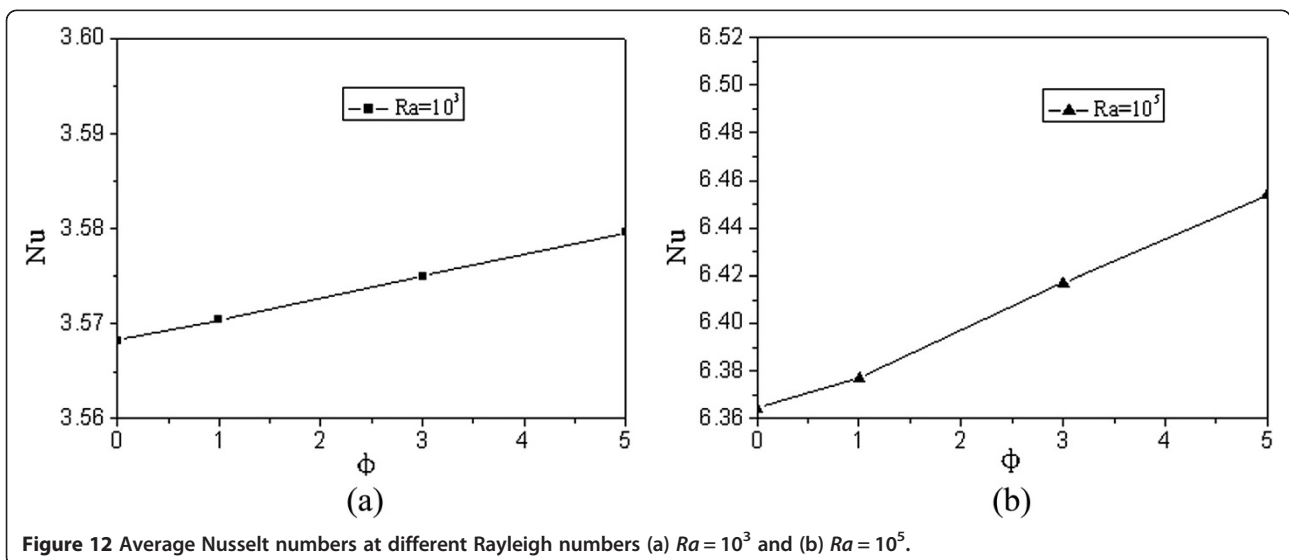

Figure 10 Nusselt number distribution along the heated surface using Al₂O₃-water nanofluid at *Ra* = 10³.

Figure 11 Nusselt number distribution along the heated surface using Al$_2$O$_3$-water nanofluid at $Ra = 10^5$.

the water-phase and nanoparticle-phase temperatures all achieve equilibrium state, the whole nanofluid (temperature distribution, velocity vectors, density distribution, and nanoparticle volume fraction distribution) is considered as being in an equilibrium state. Hence, the temperature isolines in Figures 3 and 5 look smooth due to a complete equilibrium state, and the density distribution in Figures 6 and 7 and nanoparticle volume fraction distribution in Figures 8 and 9 behave with oscillations due to an

approximate equilibrium state. Although the interparticle interaction forces have little effect on heat transfer, they play an important role on the nanoparticle distribution.

Figure 10 shows the Nusselt number distribution along the heated surface using Al$_2$O$_3$-water nanofluid at $Ra = 10^3$. It can be seen that the Nusselt number along the heated surface increases with nanoparticle volume fraction at low Y (0 < Y < 0.58) and decreases with nanoparticle volume fraction at high Y (0.58 < Y < 1). Because

Figure 12 Average Nusselt numbers at different Rayleigh numbers (a) $Ra = 10^3$ and (b) $Ra = 10^5$.

the heat transfer is more sensitive to thermal conductivity than viscosity at low Y, while it is more sensitive to viscosity than thermal conductivity at high Y.

Figure 11 shows Nusselt number distribution along the heated surface using Al_2O_3-water nanofluid at $Ra = 10^5$. It can be seen that the Nusselt number along the heated surface increases with nanoparticle volume fraction at low Y $(0 < Y < 0.875)$ and decreases with nanoparticle volume fraction at high Y $(0.875 < Y < 1)$. Compared with Figure 7, the Nusselt number becomes larger, and the enhanced heat transfer section also gets longer. The high Rayleigh number increases the velocity and then enhances the heat transfer.

Figure 12 presents the average Nusselt numbers at different Rayleigh numbers. Although the Nusselt number distribution along the heated surface increases with nanoparticle volume fraction in one section and decreases in the other section, the average Nusselt numbers at $Ra = 10^3$ and $Ra = 10^5$ both increase with nanoparticle volume fraction. For this square enclosure (left wall is kept at a high constant temperature (T_H), and top cold wall is kept at a low constant temperature (T_C)), adding nanoparticles can enhance the average heat transfer at both a low and a high Rayleigh number. In addition, the enhancement of the average Nusselt numbers is much more pronounced at a high Rayleigh number than at a low Rayleigh number.

Conclusion

A 2D two phase Lattice Boltzmann model has been developed for nanofluids and the simulation results of this two-phase Lattice Boltzmann model are in good agreement with published experimental results. This model is applied to investigate the natural convection of a square enclosure filled with Al_2O_3 nanofluid. The effects of different nanoparticle fractions and Rayleigh numbers on natural convection heat transfer of nanofluid are investigated. In addition the effects of forces on the nanoparticles volume fraction distribution and the heat transfer are also investigated.

It is found that the Nusselt number distribution along the heated surface firstly increases, and then decreases with Y at both low and high Rayleigh numbers. Average Nusselt numbers of the whole square enclosure both increase with nanoparticles volume fraction at a low and a high Rayleigh number. In addition, the enhancement of the average Nusselt numbers is much more pronounced at a high Rayleigh number than at a low Rayleigh number.

It is found that the temperature difference driving force is the biggest force and has the greatest effect on nanoparticle volume fraction distribution. For a low Rayleigh number, the nanoparticle volume fraction is low in the lower right corner and high in the top right corner and lower left corner. For a high Rayleigh number, the nanoparticle volume fraction is low at the bottom and high at the top.

Apart from the temperature difference driving force, Brownian force, interaction potential force, and gravity-buoyancy force contribute to the enhanced natural convective heat transfer, while the drag force contributes to the attenuation of heat transfer.

Nomenclature

a radius of nanoparticle (m)

A Hamaker constant

B_a weight coefficient

c reference lattice velocity

c_s lattice sound velocity

c_p specific heat capacity (J/kg K)

e_α lattice velocity vector

f_α^σ density distribution function

$f_\alpha^{\sigma eq}$ local equilibrium density distribution function

$F_\alpha^{\sigma'}$ dimensionless external force in direction of lattice velocity

F_α^σ dimensionless total interparticle interaction forces

F_S dimensionless temperature difference driving forces

F_B dimensionless Brownian force

F_H dimensionless gravity and buoyancy force

F_D dimensionless drag force

F_A dimensionless interaction potential force

g dimensionless gravitational acceleration

G dimensionless effective external force

G_i Gaussian random number

$h_{a\beta}$ convective heat transfer coefficient (W/(m^2 K))

H dimensionless characteristic length of the square cavity

k thermal conductivity coefficient (W/m/K)

k_B Boltzmann constant

L_{cc} center-to-center distance between particles (m)

Ma Mach number

m^σ mass of a single nanoparticle (kg)

n_i number of the particles within the adjacent lattice i

Nu Nusselt number

Pr Prandtl number

r position vector

Ra Rayleigh number

t time (s)

T_α^σ temperature distribution function

$T_\alpha^{\sigma eq}$ local equilibrium temperature distribution function

T dimensionless temperature

T_0 dimensionless average temperature $(T_0 = (T_H + T_C)/2)$

T_H dimensionless hot temperature

T_C dimensionless cold temperature

u^σ dimensionless macro-velocity

u_c dimensionless characteristic velocity of natural convection

V_A dimensionless interaction potential
V volume of a single lattice (m^3)
w_α weight coefficient
x, y dimensionless coordinates

Greek symbols

β^σ thermal expansion coefficient (K^{-1})
ρ^σ density (kg/m^3)
ν kinematic viscosity (m^2/s)
η dynamic viscosity (Pa s)
χ thermal diffusion coefficient (m^2/s)
γ surface tension (N/m)
ϕ nanoparticle volume fraction
δ_x lattice step
δ_t time step
σ components (σ = 1, 2, water and nanoparticles)
τ_f dimensionless collision-relaxation time for the flow field
τ_T dimensionless collision-relaxation time for the temperature field
ΔT dimensionless temperature difference
   ($\Delta T = T_H - T_C$)
$\Delta\rho'$ dimensionless mass density difference between nanoparticles and base fluid
Δu dimensionless velocity difference between nanoparticles and base fluid
$\Phi_{\alpha\beta}$ dimensionless energy exchange between nanoparticles and base fluid
Error$_1$ maximal relative error of velocities between two adjacent time layers
Error$_2$ maximal relative error of temperatures between two adjacent time layers

Subscripts

α lattice velocity direction
avg average
C cold
nf nanofluid
H hot
w base fluid
p nanoparticle

Competing interests

The authors declare that they have no competing interests.

Authors' contributions

CQ participated in the design of the program, carried out the numerical simulation of nanofluid, and drafted the manuscript. YRH conceived of the study, participated in the design of the program, and checked the grammar of the manuscript. SNY, FLT, and YWH participated in the design of the program. All authors read and approved the final manuscript.

References

1. Wang SX, Zhou Y, Guan W, Ding B: **Preparation and characterization of stimuli-responsive magnetic nanoparticles.** *Nanoscale Res Lett* 2008, **3**:289–294.
2. Bora DK, Deb P: **Fatty acid binding domain mediated conjugation of ultrafine magnetic nanoparticles with albumin protein.** *Nanoscale Res Lett* 2009, **4**:138–143.
3. Guo SZ, Li Y, Jiang JS, Xie HQ: **Nanofluids containing γ-Fe$_2$O$_3$ nanoparticles and their heat transfer enhancements.** *Nanoscale Res Lett* 2010, **5**:1222–1227.
4. Pinilla MG, Martínez E, Vidaurri GS, Tijerina EP: **Deposition of size-selected Cu nanoparticles by inert gas condensation.** *Nanoscale Res Lett* 2010, **5**:180–188.
5. Yang X, Liu Z: **A kind of nanofluid consisting of surface-functionalized nanoparticles.** *Nanoscale Res Lett* 2010, **5**:1324–1328.
6. Zhu H, Han D, Meng Z, Wu D, Zhang C: **Preparation and thermal conductivity of CuO nanofluid via a wet chemical method.** *Nanoscale Res Lett* 2011, **6**:1–6.
7. Nadeem S, Lee C: **Boundary layer flow of nanofluid over an exponentially stretching surface.** *Nanoscale Res Lett* 2012, **7**:1–6.
8. Wang L, Fan J: **Nanofluids research: key issues.** *Nanoscale Res Lett* 2010, **5**:1241–1252.
9. Oztop HF, Abu-Nada E: **Numerical study of natural convection in partially heated rectangular enclosures filled with nanofluids.** *Int J Heat Fluid Flow* 2008, **29**:1326–1336.
10. Ho CJ, Chen MW, Li ZW: **Numerical simulation of natural convection of nanofluid in a square enclosure: effects due to uncertainties of viscosity and thermal conductivity.** *Int J Heat Mass Transfer* 2008, **51**:4506–4516.
11. Saleh H, Roslan R, Hashim I: **Natural convection heat transfer in a nanofluid-filled trapezoidal enclosure.** *Int J Heat Mass Transfer* 2011, **54**:194–201.
12. Ghasemi B, Aminossadati SM: **Brownian motion of nanoparticles in a triangular enclosure with natural convection.** *Int J Therm Sci* 2010, **49**:931–940.
13. Santra AK, Sen S, Chakraborty N: **Study of heat transfer augmentation in a differentially heated square cavity using copper–water nanofluid.** *Int J Therm Sci* 2008, **47**:1113–1122.
14. Aminossadati SM, Ghasemi B: **Natural convection cooling of a localised heat source at the bottom of a nanofluid filled enclosure.** *Eur J Mech B/Fluid* 2009, **28**:630–640.
15. Kargar A, Ghasemi B, Aminossadati SM: **An artificial neural network approach to cooling analysis of electronic components in enclosures filled with nanofluids.** *J Electron Packaging* 2011, **133**:1–9.
16. Abu-Nada E, Chamkha AJ: **Effect of nanofluid variable properties on natural convection in enclosures filled with a CuO-EG-water nanofluid.** *Int J Therm Sci* 2010, **49**:2339–2352.
17. Hwang KS, Lee JH, Jang SP: **Buoyancy-driven heat transfer of water-based Al$_2$O$_3$ nanofluids in a rectangular cavity.** *Int J Heat Mass Transfer* 2007, **50**:4003–4010.
18. Jang SP, Choi SUS: **Role of Brownian motion in the enhanced thermal conductivity of nanofluids.** *Appl Phys Lett* 2004, **84**:4316–4318.
19. Barrios G, Rechtman R, Rojas J, Tovar R: **The lattice Boltzmann equation for natural convection in a two-dimensional cavity with a partially heated wall.** *J Fluid Mech* 2005, **522**:91–100.
20. Peng Y, Shu C, Chew YT: **Simplified thermal lattice Boltzmann model for incompressible thermal flows.** *Phys Rev E* 2003, **68**:026701.
21. He X, Chen S, Doolen GD: **A novel thermal model for the lattice Boltzmann method in incompressible limit.** *J Comput Phys* 1998, **146**:282–300.
22. Nemati H, Farhadi M, Sedighi K, Fattahi E, Darzi AAR: **Lattice boltzmann simulation of nanofluid in lid-driven cavity.** *Int Commun Heat Mass Transfer* 2010, **37**:1528–1534.

23. Wang J, Wang M, Li Z: **A lattice Boltzmann algorithm for fluid–solid conjugate heat transfer.** *Int J Therm Sci* 2007, **46**:228–234.
24. Dixit HN, Babu V: **Simulation of high Rayleigh number natural convection in a square cavity using the lattice Boltzmann method.** *Int J Heat Mass Transfer* 2006, **49**:727–739.
25. Peng Y, Shu C, Chew YT: **A 3D incompressible thermal lattice Boltzmann model and its application to simulate natural convection in a cubic cavity.** *J Comput Phys* 2003, **193**:260–274.
26. Xuan Y, Yao Z: **Lattice Boltzmann model for nanofluids.** *Heat Mass Transfer* 2005, **41**:199–205.
27. Russel WB, Saville DA, Schowalter WR: *Colloidal Dispersion.* Cambridge: Cambridge University Press; 1989.
28. He C, Ahmadi G: **Particle deposition in a nearly developed turbulent duct flow with electrophoresis.** *J Aerosol Sci* 1999, **30**:739–758.
29. Abu-Nada E: **Effects of variable viscosity and thermal conductivity of Al_2O_3-water nanofluid on heat transfer enhancement in natural convection.** *Int J Heat Fluid Flow* 2009, **30**:679–690.
30. Hortmann M, Peric M, Scheuerer G: **Finite volume multigrid prediction of laminar natural convection: benchmark solutions.** *Int J Numer Methods Fluid* 1990, **11**:189–207.
31. Khanafer K, Vafai K, Lightstone M: **Buoyancy-driven heat transfer enhancement in a two-dimensional enclosure utilizing nanofluids.** *Int J Heat Mass Transfer* 2003, **46**:3639–3653.
32. Krane RJ, Jessee J: **Some detailed field measurements for a natural convection flow in a vertical square enclosure.** *Proc 1st ASME-JSME Thermal Eng Joint Conf* 1983, **1**:323–329.
33. D'Orazio A, Corcione M, Celata GP: **Application to natural convection enclosed flows of a lattice Boltzmann BGK model coupled with a general purpose thermal boundary condition.** *Int J Therm Sci* 2004, **43**:575–586.
34. De Vahl DG: **Natural convection of air in a square cavity: a bench mark numerical solution.** *Int J Numer Meth Fluids* 1983, **3**:249–264.